100-Trillion-Frame-per-Second Single-Shot Compressed Ultrafast Photography via Molecular Alignment

Dalong Qi,[1] Fengyan Cao,[1] Shuwu Xu,[2] Yunhua Yao,[1] Yilin He,[1] Jiali Yao,[1] Pengpeng Ding,[1] Chengzhi Jin,[1] Lianzhong Deng,[1] Tianqing Jia,[1] Jinyang Liang,[3] Zhenrong Sun,[1,*] and Shian Zhang[1,4,5,†]

[1] *State Key Laboratory of Precision Spectroscopy, School of Physics and Electronic Science, East China Normal University, Shanghai 200062, China*

[2] *School of Sciences, Nantong University, Nantong 226007, China*

[3] *Laboratory of Applied Computational Imaging, Centre Énergie Matériaux Télécommunications, Institut National de la Recherche Scientifique, Varennes, Québec J3X1S2, Canada*

[4] *Collaborative Innovation Center of Extreme Optics, Shanxi University, Taiyuan 030006, China*

[5] *Collaborative Innovation Center of Light Manipulations and Applications, Shandong Normal University, Jinan 250358, China*

(Received 22 August 2020; revised 21 December 2020; accepted 4 February 2021; published 22 February 2021)

Compressed ultrafast photography (CUP) has the highest imaging speed and sequence depth in capturing ultrafast nonrepeatable or unstable dynamic events with snapshots. However, due to the Coulomb interaction of electrons in a streak camera, it is difficult for the imaging speed of CUP to break the speed limit of 10^{12} frames/s. Here, we propose a molecular-alignment-assisted CUP (MACUP) scheme by introducing a gas-phase temporal-spatial converter with all-optical deflection imaging into conventional CUP. Based on our simulation of a carbon dioxide molecular deflector, combined with point-spread restrictions in imaging, MACUP is able to achieve an imaging speed beyond 180×10^{12} frames/s and a sequence depth of about 300 frames in a single exposure. To demonstrate the feasibility of MACUP, we simulate the spatiotemporal intensity measurement of a chirped femtosecond laser pulse and study the image reconstruction accuracy in the intensity and wavelength evolutions. These results show that MACUP is a promising single-shot ultrafast optical imaging strategy to unravel unprecedented dynamics in ultrafast atomic and molecular optics.

DOI: 10.1103/PhysRevApplied.15.024051

I. INTRODUCTION

Single-shot ultrafast optical imaging (UOI) can acquire three-dimensional [i.e., (x, y, t)] information in nonrepeatable or difficult-to-repeat ultrafast dynamic events. To achieve this goal, the imaging speed of single-shot UOI has spanned from billions to trillions of frames per second, which is more than 5 orders of magnitude higher than that of state-of-the-art charge-coupled devices (CCDs) or complementary metal oxide semiconductor (CMOS) detectors. Therefore, single-shot UOI has attracted tremendous interest in the community of ultrafast imaging. Thus far, a few single-shot UOI methods with imaging speeds of more than 10^{12} frames/s have been proposed, including sequentially timed all-optical mapping photography [1], femtosecond time-resolved optical polarography [2,3], single-shot frequency-domain tomography [4], a frequency-recognition algorithm for multiple-exposure imaging [5], the multiple noncollinear optical parametric amplifier method [6], and compressed ultrafast photography (CUP) [7–9].

In general, snapshots of the dynamic scene at different time delays cannot be spatially overlapped in a specific domain. Otherwise, the original scene can barely be recovered correctly. However, CUP creatively synergizes the streak camera technique with compressive sensing (CS) to overcome this obstacle [10–12]. To date, it has achieved world-record imaging speeds of 10 and 70×10^{12} frames/s and sequence depths (i.e., the number of frames in one acquisition) of 350 and even over 1000 in passive and active modes, respectively [13]. Due to its outstanding performance and strong expansibility, CUP has attracted considerable attention from scientists, who have proposed a variety of variants that empower this modality, such as compressed ultrafast spectral-temporal photography [14], compressed optical-streaking ultrahigh-speed photography [15], and compressed ultrafast electron diffraction [16]

*zrsun@phy.ecnu.edu.cn
†sazhang@phy.ecnu.edu.cn

and microscopy [17]. However, as the most important element in conventional CUP, the streak camera is limited by Coulomb repulsion between photoelectrons flying with ultrahigh speeds in operation, which prevents it from achieving a temporal resolution smaller than 100 fs, even if the dynamic range is greatly sacrificed. To date, there still lacks a single-shot UOI approach to achieve an imaging speed beyond 100×10^{12} frames/s, which prevents direct observation of many transient events lasting a few hundred femtoseconds, such as the build-up process in a mode-locked ultrashort laser [18,19], femtosecond laser-induced optical phonons in condensed matters [20], and bond breaking in chemical reactions [21].

Here, we demonstrate an alternative scheme of molecular-alignment-assisted CUP (MACUP) by introducing a gas-phase temporal-spatial converter with all-optical deflection imaging into conventional CUP. We choose carbon dioxide (CO_2) as the molecular deflector and carefully simulate the deflection angle by optimizing the parameters of key elements. Furthermore, in combination with the point-spread function to find the spatial-resolution limitation at the detector, we determine the highest achievable interframe time interval of MACUP to be 5.33 fs, which means it can potentially elevate the imaging speed over 180×10^{12} frames/s. Finally, we simulate the spatiotemporal intensity measurement of a chirped femtosecond laser pulse by MACUP and analyze the imaging reconstruction accuracy in the intensity and wavelength evolutions. The simulated and reconstructed results show that MACUP is a promising single-shot UOI strategy.

II. BASIC PRINCIPLE OF MACUP

A. Image acquisition model

As a computational imaging scheme, MACUP's operation consists of data acquisition and image reconstruction. For data acquisition, the information flow is schematically illustrated in Fig. 1(a). First, the dynamic scene, $I(x, y, t)$, where x and y represent the spatial coordinates and t represents the temporal coordinate, is collected by the first imaging component (IC1) for spatially random encoding with an encoding mask. The encoding process can either be reflective [22–24] or transmissive [25]. Then, the encoded scene is relayed to a detector by IC2. A molecular deflector is inserted into the beam path to deflect the dynamic scene. Generated by an ultrashort laser pulse, molecular alignment can induce a time-varying refractive-index gradient for the temporal-to-spatial conversion of the dynamic scene. In this way, different temporal parts of the scene reach different spatial positions in the vertical direction of the detector. Finally, the encoded and sheared dynamic scene is integrated by the detector as a two-dimensional (2D) image to complete data acquisition. In this scheme, the MACUP system is designed as a passive mode. Here, the dynamic scene, the molecular deflector, and the detector (CCD) are precisely synchronized by a digital or optical delay generator.

The laser-molecule interaction scheme is shown in Fig. 1(b). A linearly polarized laser pulse, with an electric field intensity $\vec{E}$, is employed to excite a linear molecule (e.g., O_2, N_2, CO, and CO_2), and its principal axis shows an angle of θ with the orientation of $\vec{E}$. Due to the induced Kerr effect, the induced dipole moment produces rotational torque to rotate the molecule's principal axis according to the orientation of $\vec{E}$, which thus aligns the molecules. Moreover, according to the basic principle of light-beam deflection through media [26], the excitation laser beam should be rectangular. Its intensity should have a transversely uniform distribution. However, to ensure that the molecules are aligned, but not ionized, the laser pulse's peak power density has to be strictly limited between 10^{11} and 10^{13} W/cm^2 based on different kinds of molecules [27]. In addition, the laser-pulse duration can be adjusted to excite either an adiabatic or a nonadiabatic molecular alignment [28], which can be used to tune the temporal response of the molecular deflector.

B. Image reconstruction approach

Mathematically, the information flow of MACUP can be expressed as

$$E(m, n) = TSCI(x, y, t), \tag{1}$$

where $E(m, n)$ is the light-energy distribution at pixel (m, n) of the detector; C, S, and T are the spatial encoding operators representing the encoding mask, the temporal shearing operator representing the molecular deflector, and the spatiotemporal integration operator representing the CCD, respectively. Given prior knowledge of sparsity in the spatiotemporal gradient domain, the original data cube, $I(x, y, t)$, can be estimated by forming an appropriate convex objective function and solving the following optimization problem:

$$\arg\min_{I} \left\{ \frac{1}{2} ||E - TSCI||_2 + \gamma \Pi(I) \right\}. \tag{2}$$

Here, $||\ldots||_2$ denotes the l_2 norm, $\Pi(I)$ is the regularization function in the form of total variation, and γ is the regularization parameter. By utilizing appropriate algorithms, such as the two-step iterative shrinkage and thresholding (TwIST) [29] and augmented Lagrangian (AL) algorithms [30], the original dynamic scene can be recovered with high fidelity.

C. Description of the molecular deflector

Figure 1(c) shows the principle of the molecular deflector and the main parameters that determine the imaging

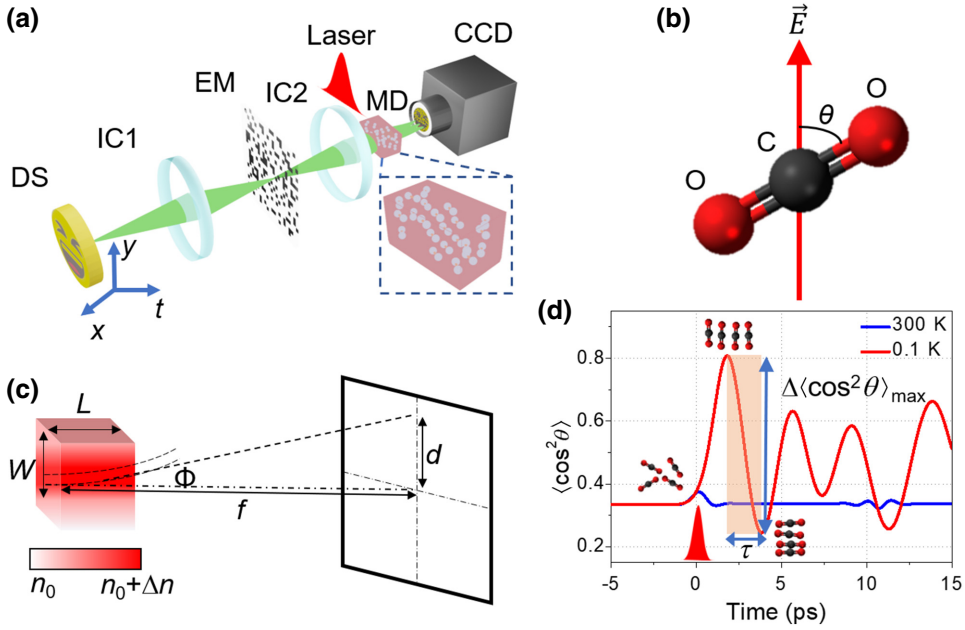

FIG. 1. (a) Schematic of data acquisition in MACUP. DS, dynamic scene; IC, imaging component; EM, encoding mask; MD, molecular deflector. (b) Principle of CO_2 molecules aligned by a laser field $\vec{E}$. (c) Molecular deflector and related parameters in MACUP. (d) Laser-induced time-resolved molecular alignment at molecular temperatures of 0.1 and 300 K.

speed of MACUP; here the maximal refractive-index gradient distribution in the molecular deflector is shown. As a huge number of molecules occupy the deflector, the degree of molecular alignment can be characterized by $\langle\cos^2\theta\rangle$ within the consideration of the Boltzmann thermal distribution [31],

$$\langle\cos^2\theta\rangle(t) = \sum_{\mathrm{J}} Q^{-1} g_J exp[-BJ(J+1)/kT] \times \sum_{M=-J}^{J} < \Psi_{JM}|\cos^2\theta|\Psi_{JM} >, \quad (3)$$

where Q, B, and J are the partition function, rotational constant, and angular momentum, respectively; g_J is the spin-degeneracy factor; and Ψ_{JM} is the rotational wave function of the time-evolved molecules. Time-dependent $\langle\cos^2\theta\rangle$ then causes a refractive-index gradient, Δn, along the excitation direction, which can be expressed by

$$\Delta n(\omega) = \frac{2\pi N_0}{n_0}\Delta\alpha\Delta\langle\cos^2\theta\rangle, \quad (4)$$

where $N_0 = p/RT$ is the molecular density under the ideal gas equation of state; p, R, and T are pressure, gas constant, and temperature, respectively; $\Delta\alpha$ represents the difference between the parallel and perpendicular polarizabilities of a molecule; $\Delta\langle\cos^2\theta\rangle$ represents the largest difference of molecular-alignment degree in a linear change of refractive-index gradient; and n_0 denotes the initial refractive index. The dynamic scene can be deflected within an angle of Φ, when passing through the molecular deflector [see Fig. 1(c)]. Here, the length and width of the deflector are set as L and W, respectively. A depth displacement, s, is also caused if the dynamic scene is shifted by a maximal distance of d on the detector. Assuming that the elementary pixel size of the CCD is Δd, the sequence depth can be easily determined by $N = d/\Delta d + 1$, on account of the basic principle of MACUP. The interframe time interval can be formulated as $\Delta t = (\sqrt{2}/2)\tau/N$, in which $\sqrt{2}/2$ originates from the approximation of the linear part in a sinusoidal curve, and τ is the time width that $\Delta\langle\cos^2\theta\rangle_{\max}$ occurs in a quasilinear change.

To search for optimal values of the interframe time interval and corresponding sequence depth, a few preconditions have to be met. On one hand, since a dynamic scene has to experience a quasilinear change during propagation through the molecular deflector, $W = (\sqrt{2}/2)\tau c$ is chosen to provide the transversal region for the time-varying refractive-index gradient, in which c is the speed of light. In addition, $L < W$ should be satisfied, since the dynamic scene has to be within this period during propagation through the molecular deflector. On the other hand, the point-spread restriction through a circular aperture also has to be taken into consideration for imaging [32]. According to the oscillation timescale of molecules, the entrance pupil of MACUP is limited by W on the scale of a few hundred micrometers; therefore, within the consideration of no pixel binning, $f = W\Delta d/(1.22\lambda)$ has to be obeyed, where λ denotes to the central wavelength of the dynamic scene. Based on these preconditions, the interframe time interval

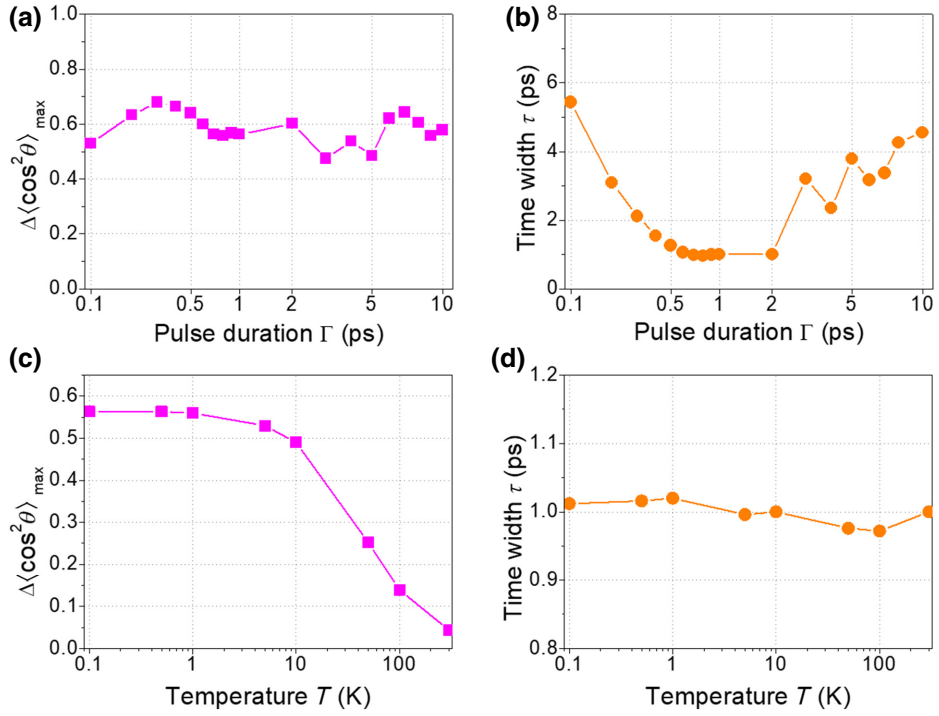

FIG. 2. $\Delta\langle\cos^2\theta\rangle_{max}$ (a) and time width τ (b) varying with laser-pulse duration Γ at a molecular temperature of 0.1 K. $\Delta\langle\cos^2\theta\rangle_{max}$ (c) and time width τ (d) varying with molecular temperature T for a laser-pulse duration of 300 fs.

(i.e., the reciprocal of the imaging speed) of MACUP can thus be expressed by

$$\Delta t = \frac{1.22\lambda}{c\tan[(L/W)(2\pi p/RTn_0)\Delta\alpha\Delta < \cos^2\theta >_{max}]}. \quad (5)$$

Meanwhile, the sequence depth is given by

$$N = \frac{d}{\Delta d} = \frac{\sqrt{2}\tau c\tan[(L/W)(2\pi p/RTn_0)\Delta\alpha\Delta < \cos^2\theta >_{max}]}{2.44\lambda}. \quad (6)$$

It can be concluded from Eqs. (5) and (6) that both Δt and N are jointly determined by a few parameters, including λ, L/W, T, $\Delta\alpha$, and $\Delta\langle\cos^2\theta\rangle_{max}$. N is only positively proportional to τ and not Δt. To achieve an imaging speed as high as possible, all of the parameters are analyzed in detail to minimize Δt, and the corresponding N is also given to ensure a sufficient number of frames to recover. First, $\lambda = 550$ nm is chosen for typical visible dynamic scenes. It is worth noting that there may be a difference in the phase velocity and group velocity between the dynamic scenes due to the spectral span, but it can be restrained via precompensation in the image reconstruction, according to spectral information. Second, a larger L/W can induce a larger deflection angle, but the temporal duration of the dynamic scene that can be captured is restricted. Thus, the value is set at 0.9. Third, assuming that p is kept unchanged, while T varies, a lower temperature is critical for both specifications. Moreover, it can be seen from Eq. (3) that a lower temperature can cause a larger $\Delta\langle\cos^2\theta\rangle_{max}$, which also contributes to improving Δt and N. Last, but not least, $\Delta\alpha$ shows a huge difference between molecules. CO_2 is selected, since it holds a rather high $\Delta\alpha$ value that is over 2 times larger than that of other common molecules [33].

III. OPTIMIZATION OF MACUP PERFORMANCE

A. Optimization of deflector parameters

To intuitively explore the optimal imaging performance of MACUP, a Gaussian laser pulse centered at 800 nm, with 1 ps pulse duration, is first employed to excite CO_2 molecules at molecular temperatures of 0.1 and 300 K, and the time-resolved response of $\langle\cos^2\theta\rangle$ is shown in Fig. 1(d). It can be seen that a nonadiabatic alignment is generated after laser excitation. The molecules in the molecular deflector align more in parallel or perpendicular to the orientation of $\vec{E}$ when the value is larger or smaller than 1/3, respectively. Specifically, $\Delta\langle\cos^2\theta\rangle_{max}$, along with the corresponding time width τ, are responsible for the temporal

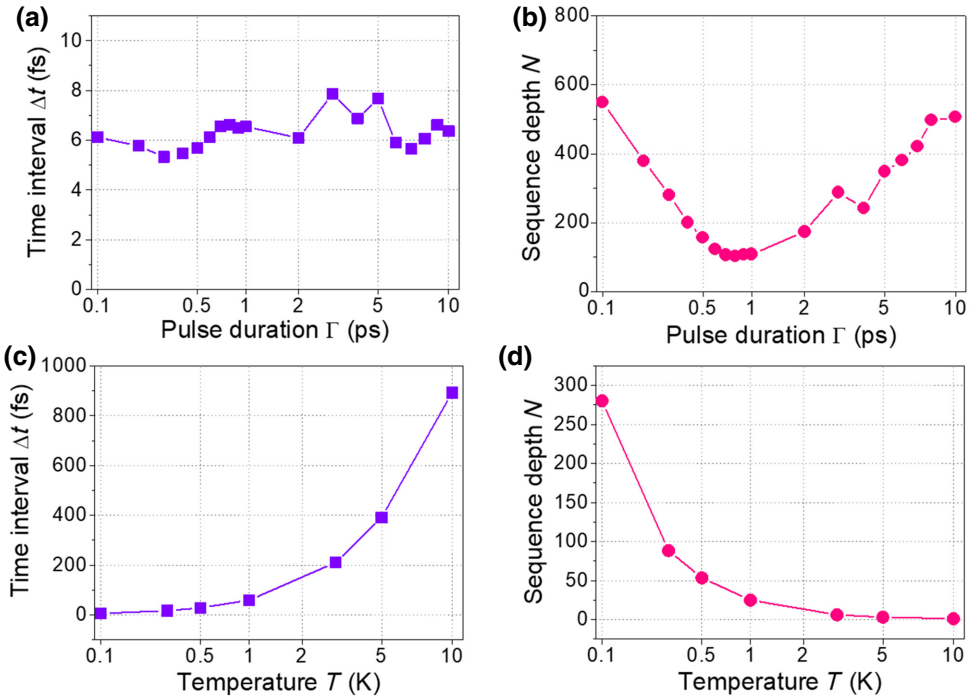

FIG. 3. Interframe time interval Δt (a) and sequence depth N (b) varying with laser-pulse duration Γ at a molecular temperature of 0.1 K. Interframe time interval Δt (c) and sequence depth N (d) varying with molecular temperature T for a laser-pulse duration of 300 fs.

response of the molecular deflector. Moreover, this difference is rather small for deflection at 300 K, but a molecular temperature as low as 0.1 K can enlarge it by over 10 times, which is beneficial for superior imaging performance.

The dependences of molecular alignments on laser-pulse durations, Γ, and molecular temperatures, T, are simulated based on the excitation conditions of Fig. 1(d). First, $\Delta\langle\cos^2\theta\rangle_{\max}$ and τ are excited by laser-pulse durations from 0.1 to 10 ps at a molecular temperature of 0.1 K, A shown in Figs. 2(a) and 2(b), respectively. It can be seen that $\Delta\langle\cos^2\theta\rangle_{\max}$ shows a fluctuation at around 0.6 with increasing laser-pulse duration, while a maximum of about 0.68 appears with 300 fs laser excitation. All of these results indicate that the molecular-alignment degree is rather high for beam deflection. Meanwhile, τ first decreases and then increases. It reaches a minimum value of about 1 ps with a pulse duration of 700 fs. When the pulse duration is more than 2 ps, τ shows an oscillation, which may be due to competition between adiabatic and nonadiabatic processes. Additionally, both $\Delta\langle\cos^2\theta\rangle_{\max}$ and τ, excited at molecular temperatures from 0.1 to 300 K, are mapped in Figs. 2(c) and 2(d), respectively. The lower temperatures favor a large $\Delta\langle\cos^2\theta\rangle_{\max}$. A plateau is seen at about 0.56 when T is below 1 K, while it drops vastly with a further increase of the molecular temperature to less than 0.1 at 300 K. For τ, it fluctuates around 1 ps throughout the molecular-temperature range, which indicates that the molecular temperature has almost no effect on τ.

B. Optimization of imaging performance

Accordingly, the effects of the laser-pulse duration and molecular temperature on the interframe time interval, Δt, and sequence depth, N, of MACUP can be determined by Eqs. (5) and (6), and the results are shown in Fig. 3. The dependences of Δt and N on the laser-pulse durations at 0.1 K are shown in Figs. 3(a) and 3(b), respectively. As shown in Eq. (5), Δt is inversely proportional to $\Delta\langle\cos^2\theta\rangle_{\max}$ within the small-angle approximation. Therefore, similar to $\Delta\langle\cos^2\theta\rangle_{\max}$ in Fig. 2(a), Δt also shows a fluctuation, but it is always smaller than 8 fs, which corresponds to an imaging speed of more than 125×10^{12} frames/s. Moreover, as shown in Eq. (6), N is approximately proportional to τ, while it is inversely proportional to $\Delta\langle\cos^2\theta\rangle_{\max}$. Since the laser-pulse duration has little effect on $\Delta\langle\cos^2\theta\rangle_{\max}$, N has the same evolution behavior as τ, i.e., a decrease followed by an increase with longer laser-pulse durations. Notably, the highest interframe time interval reaches 5.33 fs with 300 fs laser excitation, and the corresponding N is about 300; both of these values sufficiently qualify for single-shot UOI. Moreover, we simulate the two parameters Δt and N by varying the molecular temperature for determining experimental guidelines, as shown in Figs. 3(c) and 3(d), respectively. It can be concluded that, at a higher temperature, worse Δt and poorer N are achieved. Even worse, N decreases almost exponentially with increasing molecular temperature and is less than 50 frames at 1 K, which means that a rather low operation temperature of less than 1 K is

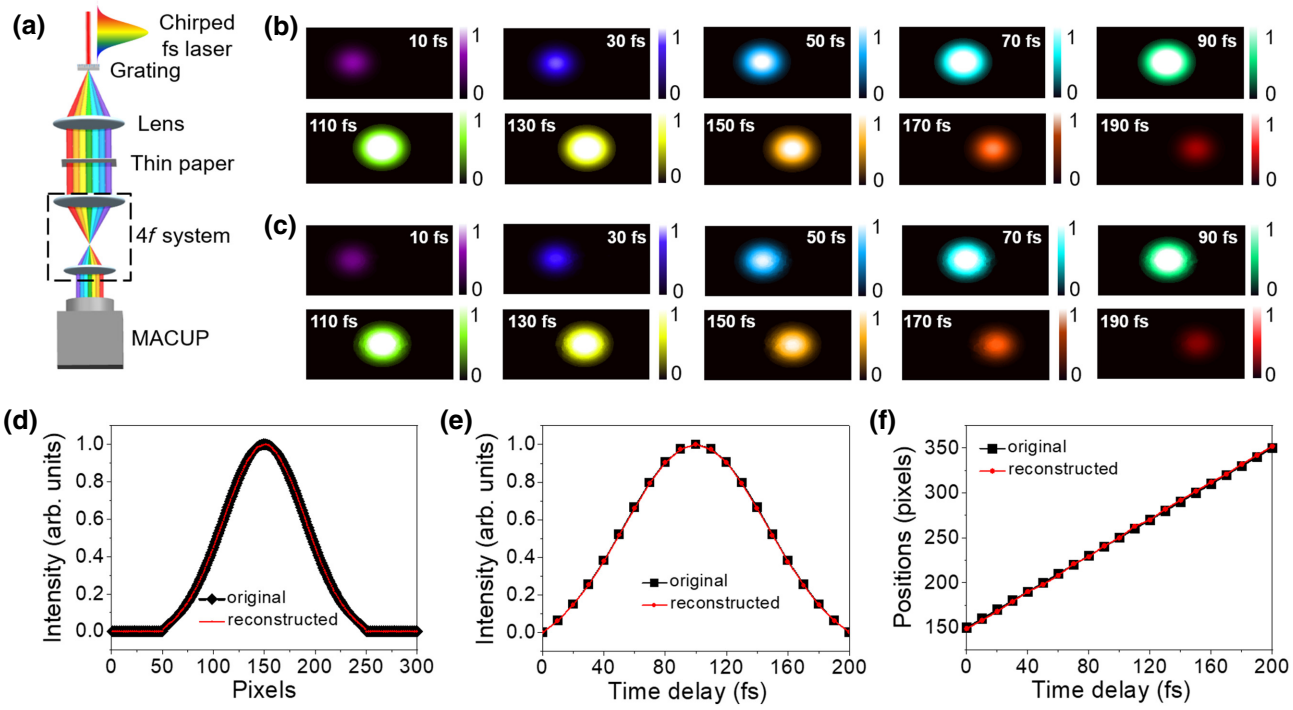

FIG. 4. (a) Experimental design of the spatiotemporal intensity measurement of a chirped femtosecond laser pulse. Selected original (b) and reconstructed (c) images of laser-spot evolution. Intensity profiles of the tenth frame (d), time-resolved intensities (e), and time-resolved positions (f) extracted from the original (squares) and reconstructed (circles) images.

indispensable to realize a credible imaging performance of MACUP via CO_2.

IV. CHIRPED FEMTOSECOND-LASER-PULSE PROPAGATION SIMULATION

As a computational imaging strategy assisted by CS, the quality of image reconstruction in MACUP is as important as data acquisition. Fortunately, CS algorithms have shown powerful reconstruction abilities in a series of studies [34]. Here, a simulated spatiotemporal intensity measurement of a chirped femtosecond laser pulse is recovered by the AL algorithm to validate the reconstruction performance. A temporally chirped femtosecond laser pulse with a Gaussian intensity distribution in time and space is spatially dispersed by a transmissive grating, then the chirped femtosecond laser spot is projected on thin white paper, and a small fraction of photons pass through it; thus, the spatiotemporal intensity evolution of the chirped femtosecond laser pulse is captured by MACUP after passing through a $4f$ imaging system, as shown in Fig. 4(a). Therefore, the short-wavelength components lead the laser pulse, while the long-wavelength components are in the tail. Moreover, the laser spot shifts in position along the dispersing direction, which indicates that the wavelength components of the chirped femtosecond laser pulse can be spatially resolved. We consider that the whole temporal profile of the laser spot from appearance to disappearance is 200 fs, and 21 frames of images with a 10 fs time interval, representing spatiotemporal intensity evolution, are employed. In our simulation, all of the images are randomly encoded, shift sequentially, and are superimposed to form a single 2D image for image reconstruction. The selected original and reconstructed images of the chirped-laser-pulse evolution are shown in Figs. 4(b) and 4(c), respectively. As can be seen, the globally normalized signals in Fig. 4(c) retain the highly reliable evolution behavior of the original scene, except for slight blurring at the edges of the beam. To quantitatively evaluate the reconstruction performance, we first extract the intensity distributions of the original and reconstructed laser-beam snapshot along the vertical direction in the tenth frame, as shown in Fig. 4(d). It is observed that the recovered laser beam's intensity profile, as well as the central position, are almost coincident with that of the original one, showing that both the spatial profile and position of the beam in an individual frame are reliably reconstructed. Furthermore, the intensity and position evolutions extracted under both circumstances are shown in Figs. 4(e) and 4(f), respectively. The intensity of the laser beam in each frame is accumulated and globally normalized, as shown in Fig. 4(e). It can be seen that the reconstructed intensity evolution is very similar to that of the original signal, illustrating that the Gaussian-shape intensity dynamics during dispersion is finely retained.

Similarly, Fig. 4(f) shows that the reconstructed central positions of different wavelength components are highly consistent with those of the original ones. All simulation results of the chirped femtosecond laser-pulse evolution reveal that the reconstruction algorithm for MACUP is competent for recovering ultrafast dynamics with high quality, and there are reasons to believe that more reliable images will be reconstructed in combination with deep-learning strategies [35].

V. CONCLUSIONS AND PERSPECTIVES

We theoretically establish a single-shot CUP modality via molecular alignment. A CO_2 molecular deflector is designed to realize all-optical deflection imaging in a conventional CUP system. By constructing the theoretical model of MACUP and optimizing the key parameters, rather high imaging speeds beyond 180×10^{12} frames/s, and corresponding sequence depths, are determined for the guidance of experimental realization. In addition, the simulated spatiotemporal intensity measurement of a chirped femtosecond laser pulse is validly reconstructed by an AL algorithm. According to our simulation, the pivotal parameters that determine the imaging performance of MACUP are the time-response function of the molecular deflector and the deflection angle. Compared with those techniques based on acousto- and electro-optical deflection strategies, the molecular deflectors can have a response as short as a few picoseconds. Furthermore, the deflection angle can effectively increase with the assistance of cryogenic techniques. Based on the two advantages and existing experimental conditions, our proposed MACUP scheme is completely feasible in experiments. It is expected that MACUP with ultrahigh imaging speeds will be capable of unraveling unprecedented dynamics in ultrafast atomic and molecular optics.

ACKNOWLEDGMENTS

This work is partially supported by the National Natural Science Foundation of China (Grants No. 91850202, No. 12074121, No. 11774094, No. 11804097, No. 11727810, and No. 12034008) and the Science and Technology Commission of Shanghai Municipality (Grants No. 19560710300 and No. 20ZR1417100).

D. Di and F. Cao contributed equally to this work. D.Q., S.Z., and Z.S. conceived the idea and designed the research. D.Q. and F.C. conducted most of the simulations and drafted the manuscript. S.X. performed the molecular alignment simulation. Y.Y., Y.H., J.Y., P.D., and C.J. contributed to the CUP-related simulation. L.D., T.J., and J.L. contributed to the project optimization and revised the manuscript. All authors contributed to the discussion of the paper.

The authors declare that they have no conflict of interest.

[1] K. Nakagawa, A. Iwasaki, Y. Oishi, R. Horisaki, A. Tsukamoto, A. Nakamura, K. Hirosawa, H. Liao, T. Ushida, K. Goda, et al., Sequentially timed all-optical mapping photography (STAMP), Nat. Photonics **8**, 695 (2014).

[2] M. Fujimoto, S. Aoshima, M. Hosoda, and Y. Tsuchiya, Femtosecond time-resolved optical polarigraphy: Imaging of the propagation dynamics of intense light in a medium, Opt. Lett. **24**, 850 (1999).

[3] X. Wang, L. Yan, J. Si, S. Matsuo, H. Xu, and X. Hou, High-frame-rate observation of single femtosecond laser pulse propagation in fused silica using an echelon and optical polarigraphy technique, Appl. Opt. **53**, 8395 (2014).

[4] Z. Li, R. Zgadzaj, X. Wang, Y. Y. Chang, and M. C. Downer, Single-shot tomographic movies of evolving light-velocity objects, Nat. Commun. **5**, 3085 (2014).

[5] A. Ehn, J. Bood, Z. Li, E. Berrocal, M. Aldén, and E. Kristensson, FRAME: Femtosecond videography for atomic and molecular dynamics, Light: Sci. Appl. **6**, e17045 (2017).

[6] X. Zeng, S. Zheng, Y. Cai, Q. Lin, J. Liang, X. Lu, J. Li, W. Xie, and S. Xu, High-spatial-resolution ultrafast framing imaging at 15 trillion frames per second by optical parametric amplification, Adv. Photonics **2**, 056002 (2020).

[7] L. Gao, J. Liang, C. Li, and L. V. Wang, Single-shot compressed ultrafast photography at one hundred billion frames per second, Nature **516**, 74 (2014).

[8] J. Liang, C. Ma, L. Zhu, Y. Chen, L. Gao, and L. V. Wang, Single-shot real-time video recording of a photonic Mach cone induced by a scattered light pulse, Sci. Adv. **3**, e1601814 (2017).

[9] J. Liang, L. Zhu, and L. V. Wang, Single-shot real-time femtosecond imaging of temporal focusing, Light: Sci. Appl. **7**, 42 (2018).

[10] Guide to streak cameras. https://www.hamamatsu.com/resources/pdf/sys/SHSS0006E_STREAK.pdf [accessed 26-May-2020].

[11] R. M. Willett, R. F. Marcia, and J. M. Nichols, Compressed sensing for practical optical imaging systems: A tutorial, Opt. Eng. **50**, 072601 (2011).

[12] J. Liang, Punching holes in light: Recent progress in single-shot coded-aperture optical imaging, Rep. Prog. Phys. **83**, 116101 (2020).

[13] P. Wang, J. Liang, and L. V. Wang, Single-shot ultrafast imaging attaining 70 trillion frames per second, Nat. Commun. **11**, 2091 (2020).

[14] Y. Lu, T. T. Wong, F. Chen, and L. Wang, Compressed Ultrafast Spectral-Temporal Photography, Phys. Rev. Lett. **122**, 193904 (2019).

[15] X. Liu, J. Liu, C. Jiang, F. Vetrone, and J. Liang, Single-shot compressed optical-streaking ultra-high-speed photography, Opt. Lett. **44**, 1387 (2019).

[16] D. Qi, C. Yang, F. Cao, J. Liang, Y. He, Y. Yang, T. Jia, Z. Sun, and S. Zhang, Compressed Ultrafast Electron Diffraction Imaging Through Electronic Encoding, Phys. Rev. Appl. **10**, 054061 (2018).

[17] X. Liu, S. Zhang, A. Yurtsever, and J. Liang, Single-shot real-time sub-nanosecond electron imaging aided by compressed sensing_analytical modeling and simulation, Micron **117**, 47 (2019).

[18] G. Herink, B. Jalali, C. Ropers, and D. R. Solli, Resolving the build-up of femtosecond mode-locking with single-shot

spectroscopy at 90 MHz frame rate, Nat. Photonics **10**, 321 (2016).

[19] J. Peng, M. Sorokina, S. Sugavanam, N. Tarasov, D. V. Churkin, S. K. Turitsyn, and H. Zeng, Real-time observation of dissipative soliton formation in nonlinear polarization rotation mode-locked fibre lasers, Commun. Phys. **1**, 20 (2018).

[20] T. Ishikawa, S. A. Hayes, S. Keskin, G. Corthey, M. Hada, K. Pichugin, A. Marx, J. Hirscht, K. Shionuma, K. Onda, et al., Direct observation of collective modes coupled to molecular orbital-driven charge transfer, Science **350**, 1501 (2015).

[21] A. H. Zewail, Femtochemistry: Atomic-scale dynamics of the chemical bond, J. Phys. Chem. A **104**, 5660 (2000).

[22] C. Yang, F. Cao, D. Qi, Y. He, P. Ding, J. Yao, T. Jia, Z. Sun, and S. Zhang, Hyperspectrally Compressed Ultrafast Photography, Phys. Rev. Lett. **124**, 023902 (2020).

[23] C. Yang, D. Qi, F. Cao, Y. He, J. Yao, P. Ding, X. Ouyang, Y. Yu, T. Jia, S. Xu, Z. Sun, and S. Zhang, Single-shot Receive-Only Ultrafast Electro-Optical Deflection Imaging, Phys. Rev. Appl. **13**, 024001 (2020).

[24] F. Cao, C. Yang, D. Qi, J. Yao, Y. He, X. Wang, W. Wen, J. Tian, T. Jia, Z. Sun, and S. Zhang, Single-shot spatiotemporal intensity measurement of picosecond laser pulses with compressed ultrafast photography, Opt. Laser Eng. **116**, 89 (2019).

[25] J. Yao, D. Qi, C. Yang, F. Cao, Y. He, P. Ding, C. Jin, Y. Yao, T. Jia, Z. Sun, and S. Zhang, Multichannel-coupled compressed ultrafast photography, J. Opt. **22**, 085701 (2020).

[26] V. J. Fowler and J. Schlafer, A survey of laser beam deflection techniques, Appl. Optics **5**, 1675 (1966).

[27] C. P. Koch, M. Lemeshko, and D. Sugny, Quantum control of molecular rotation, Rev. Mod. Phys. **91**, 035005 (2019).

[28] J. Omiste, M. Gärttner, P. Schmelcher, R. González-Férez, L. Holmegaard, J. Nielsen, H. Stapelfeldt, and J. Küpper, Theoretical description of adiabatic laser alignment and mixed-field orientation: The need for a non-adiabatic model, Phys. Chem. Chem. Phys. **13**, 18815 (2011).

[29] J. M. Bioucas-Dias and M. A. T. Figueiredo, A new TwIST: Two-step iterative shrinkage/ thresholding algorithms for image restoration, IEEE Trans. Image Process **16**, 2992 (2007).

[30] C. Yang, D. Qi, F. Cao, Y. He, X. Wang, W. Wen, J. Tian, T. Jia, Z. Sun, and S. Zhang, Improving the image reconstruction quality of compressed ultrafast photography via an augmented Lagrangian algorithm, J. Opt. **21**, 035703 (2019).

[31] S. Zhang, C. Lu, J. Shi, T. Jia, Z. Wang, and Z. Sun, Field-free molecular alignment by shaping femtosecond laser pulse with cubic phase modulation, Phys. Rev. A **84**, 013408 (2011).

[32] D. E. Stoltzmann, The perfect point spread function, Appl. Opt. and Opt. Eng. **9**, 111 (1983).

[33] C. H. Lin, J. P. Heritage, T. K. Gustafson, R. Y. Chiao, and J. P. McTague, Birefringence arising from the reorientation of the polarizability anisotropy of molecular in collisionless gases, Phys. Rev. A **13**, 813 (1976).

[34] D. Qi, S. Zhang, C. Yang, Y. He, F. Cao, J. Yao, P. Ding, L. Gao, T. Jia, J. Liang, Z. Sun, and L. V. Wang, Single-shot compressed ultrafast photography: A review, Adv. Photonics **2**, 014003 (2020).

[35] Y. Ma, X. Feng, and L. Gao, Deep-learning-based image reconstruction for compressed ultrafast photography, Opt. Lett. **45**, 4400 (2020).